QUANTUM CASCADE LASER-ASSISTED TIME-RESOLVED MEASUREMENTS OF CARBON DIOXIDE ABSORPTION DURING COMBUSTION IN DME-HCCI ENGINE

Ulugbek Azimov[a,*], Nobuyuki Kawahara[b], Eiji Tomita[b]

[a]*Department of Mechanical and Construction Engineering, University of Northumbria, City campus, Newcastle upon Tyne, NE1 8ST, United Kingdom*
[b]*Department of Mechanical Engineering, Okayama University, Tsushima-Naka 3, Okayama 700-8530, Japan*

Abstract

We conducted experiments to investigate in-cylinder light absorption by carbon dioxide (CO_2) during homogeneous charge compression ignition (HCCI) engine combustion. The combustion was fuelled with dimethyl ether. An *in situ* laser infrared absorption method was developed. We used an optical fibre spark plug sensor and the light source was a 4.301 μm quantum cascade laser (QCL). We applied Lambert–Beer's law in the case of a single absorption line of CO_2. We were able to measure the transient CO_2 formation during the HCCI combustion inside the engine cylinder. Our experiments showed that the laser light transmissivity level decreased with the intensity of the infrared (IR) signal. We compared the change in the transmissivity to the spatially integrated HCCI flame luminosity level and observed significant correlations between the flame luminosity level, heat release rate and transmissivity. Time-resolved experiments showed that the CO_2 absorbance increases when the second peak of the rate of heat release (ROHR) is maximised. After combustion, the CO_2 concentration was approximately 4 vol. %, which agrees with the amount of CO_2 formed during complete combustion.

Keywords: HCCI; IC engine combustion; dimethyl ether; CO_2 infrared light absorption; heat release rate; quantum cascade laser

1. Introduction

Homogeneous charge compression ignition (HCCI) engines have received much attention due to their high combustion efficiency and low nitrogen oxide (NOx) and particulate matter (PM) emission rates. Recent studies on HCCI-based combustion engines have focused on four-stroke engines using conventional or alternative fuels, including dimethyl ether (DME) fuel [1-4]. In HCCI engines, DME fuel exhibits very strong low-temperature kinetic reactions, making it suitable for compression ignition engines. It is a promising alternative fuel due to the fact that it will not contribute to the air-pollution problems caused by soot and NOx [5], which are emitted by conventional fuels. To improve understanding of the DME oxidation mechanism in an HCCI engine, we conducted experimental kinetic studies to characterise the combustion. One effective way to investigate the DME reaction mechanisms is to use spectral analysis to determine the major active species, especially CO_2 and CO [6-9]. A number of studies have examined CO_2 and CO absorption in a constant volume vessel or reactor. However, few studies have examined CO_2 formation and absorption under normal engine conditions. Schultz et al. [10] investigated the impact of ultraviolet (UV) absorption by CO_2 in high-pressure combustion applications. They measured the absorption cross section of CO_2 at combustion temperatures corresponding to wavelengths of 190 nm and found that the measured absorption cross section had a pronounced temperature dependence in the case of CO_2, and that to analyse the absorption by hot combustion products, significant corrections to the UV combustion measurements must be made. Farooq et al. [11] performed high-pressure measurements of CO_2 absorption at wavelengths near 2.7 μm. They concluded that in this wavelength range, as the spectra broaden and blend at high densities, access to discrete transitions is not possible. This makes it difficult to avoid H_2O interference. Hall et al. [12] used broadband infrared radiation from a tungsten halide lamp to analyse the density of CO_2 in the cylinder of a spark-ignited (SI) engine. The CO_2 was measured by the attenuation of the infrared radiation, which occurs due to the excitation of the 2,300cm^{-1} infrared vibrational–rotational absorption band. Kawahara et al. [13] used infrared laser absorption to conduct cycle-resolved residual gas concentration measurements inside a heavy-duty diesel engine. They were able to quantify the CO_2 concentration in the residual gas and estimate the internal exhaust gas recirculation (EGR) ratio. Residual gas concentrations, especially CO_2 and H_2O, have also been measured *in situ* using infrared absorption techniques [14, 15]. Francqueville et al. [15] measured the CO_2 concentration across the combustion chamber in a spark-ignited engine. Grosch et al. [16] performed infrared spectroscopic concentration measurements of CO_2 and gaseous H_2O in environments that are difficult to measure directly using a fibre optical sensor. The mixture of CO_2 and H_2O was analysed spectrally at a wavelength of about 3,700cm^{-1} for temperatures up to 573 K and pressures up to 1,800 kPa. An optical absorption sensor was used to make quantitative in-cylinder transmission measurements.

Optical absorption-based sensors are used to analyse mixture formation in spark-ignited engines. Using these sensors, it is possible to access the cylinder without modifications such as optical windows. As a result, the thermodynamic and mechanical properties of the engine being studied will not be changed by the apparatus, enabling measurements to be made under realistic conditions. The in-cylinder mixture was analysed using optical absorption-based sensors in conjunction with gas sampling probes. Little progress has been made towards the development of practical absorption-based sensors for CO_2 measurements in high-pressure combustion environments. Most previous high-pressure CO_2 sensors used robust telecommunications diode lasers and optical fibre technology in the near-infrared (NIR) 1.3–1.6 μm wavelength region. These sensors accessed weak vibrational bands of CO_2 by direct absorption [22] and used direct absorption spectroscopy [17–19], wavelength modulation spectroscopy (WMS) [20, 21], or NIR hyperspectral sources. To explore the challenges of optical sensor design for high-pressure applications [23], high-pressure measurements of CO_2 absorption have recently been performed near 2.0 μm.

The work presented in this paper is motivated by the need for an *in-situ* absorption-based diagnostic for measuring transient CO_2 concentrations in HCCI engine cylinders. Understanding the transient CO_2 formation process may help resolve problems related to knocking combustion [24] and exhaust gas formation [25]. This also aids the design of efficient HCCI engines with precise ignition timing control and a variable valve timing system [26, 27]. The objective of this study was to measure transient CO_2 formation during DME-HCCI combustion. By combining spectroscopy and QCLs, we were able to determine the CO_2 light absorption. Our aim was to characterise the time-resolved spectrum of CO_2 formation. CO_2 formation is a representative indicator of thermal ignition and fuel oxidation during HCCI combustion.

2. Experimental setup and procedure

We used an optical compression–expansion test engine with a single cylinder and a compression ratio of 9.0, as shown in Figure 1 and Table 1, to study DME-fuelled HCCI. The engine crank was driven externally by a 2,000 W induction motor and rotated at a constant rate of 600 rpm. The DME was premixed with gas at a ratio of 20% oxygen to 80% argon at molar proportions equivalent to $\phi = 0.30$. Argon was used instead of nitrogen for two reasons: firstly, to increase the in-cylinder temperature at the end of compression by decreasing the heat capacity of the in-cylinder gas–fuel mixture; and secondly, to initiate HCCI combustion at a significantly lower compression ratio than that used in conventional HCCI engines. The DME–O_2–Ar fuel mixture was supplied to the mixture tank, where it was heated to the temperature T_{in}= 293 K, 303 K and 310 K and maintained at pressure P_{in} = 65 kPa. While the motor was on, the intake valve remained open, and the fuel mixture was sucked into the cylinder and pushed back into the mixture tank. When the thermocouple reading in the mixture tank stabilised, a valve closure signal was sent to a solenoid that activated the valve stopper. The intake valve was closed at around bottom dead centre (BDC), and the fuel mixture was compressed, autoignited, and combusted. Changes in the gas pressure were measured during the compression and expansion strokes using a KISTLER 6052B pressure transducer. Concurrently, sequential HCCI-DME combustion images were recorded by a high-speed camera (MEMRECAM GX-8; Nac Image Technology Inc., Simi Valley, CA, USA) at 10,000 frames per second with a resolution of 640 × 640 pixels. CO_2 absorption was measured by directing laser light from the QCL to the spark plug sensor via optical fibres, and then to the infrared (IR) detector. A QCL is a semiconductor laser that emits light in the mid- to far-infrared portion of the electromagnetic spectrum. Unlike typical interband semiconductor lasers, which emit electromagnetic radiation through the recombination of electron–hole pairs across the material band gap, the QCL is unipolar and laser emission is achieved via intersubband transitions in a repeated stack of semiconductor multiple quantum well heterostructures [28]. A QCL was used as the light source due to its strong absorption, and because no other gas needs to be introduced to the burned gas or fresh mixture. The centre-wavelength of the QCL at 4.301 μm, shown in Figure 2, coincides with the absorption line of CO_2. This absorption line is caused by the C–O vibrational-rotational band, estimated using the HITRAN database to occur at temperature 900K [29]. The temperature of 900 K is typical in the combustion conditions investigated. Figure 3 shows an optical fibre-embedded spark plug installed into an engine cylinder head (A). The spark plug includes an electrode and a metallic mirror for laser beam reflection. A schematic diagram of the optical spark plug is shown in (B). The light was transmitted through an optical fibre to the spark-plug sensor installed in the combustion chamber and reflected back from the metal mirror of the sensor, passing through an optical fibre again, and finally to the IR detector (P4631; Hamamatsu Photonics K.K., Hamamatsu, Japan), as shown in Figure 1. A band-pass filter with a centre-wavelength of 4.300 μm and full-width at half-maximum (FWHM) of 160 nm was placed in front of the IR detector.

The infrared spectral absorbance was determined by applying the Lambert-Beer law to the measured spectral transmission. The Lambert-Beer law relates the attenuation of light to the properties of the material through which the light is traveling. The proportion of the light absorbed will depend on how many molecules it interacts with.

$$A(\lambda) = \log_{10}\left[\frac{I_0(\lambda)}{I(\lambda)}\right] = \varepsilon c L \tag{1}$$

where $A(\lambda)$ is the spectral absorbance, $I_0(\lambda)$ is the intensity in an air-filled environment, $I(\lambda)$ is the intensity in a DME–O_2–Ar-filled environment, and ε, c and L are the molar absorption coefficient, molar concentration, and measurement length, respectively. To use this law, the molar absorption coefficient of the CO_2 was determined for different pressures and temperatures in advance. In our test engine experiments, we simultaneously measured the CO_2 absorption and in-cylinder pressure, and made a high speed camera recording of the combustion. The initial conditions were fixed at P_{in} = 65 kPa, T_{in} = 293, 303 and 310 K, ϕ = 0.3. Taking into account cyclic variations in the in-cylinder combustion, the resultant combustion intensities were defined as weak, medium and strong. These combustion intensities were defined as the rate of maximum pressure rise with respect to the crank angle. Figure 4 shows the distribution of the maximum pressure rise for different combustion cycles. Weak combustion cycles have a value below 0.05 MPa/dθ. Just above this level, there are a few medium-intensity combustion cycles, followed by a large distribution of high-intensity combustion cycles. We determined correlations between the combustion intensity, in-cylinder pressure, ROHR and time-resolved CO_2 absorption.

3. **Results and discussion**

3.1 IR signal and laser light transmissivity

To ensure a valid analysis, we must take particular care because the pressure and temperature inside the engine cylinder change drastically as the piston moves. The purpose of this study was to quantify the history of the CO_2 concentration inside the combustion chamber; therefore, the molar absorption coefficient of the CO_2 had to be determined in advance at different pressures and temperatures. Figure 5 shows an example of the effects of the ambient pressure and temperature on the molar absorption coefficient of CO_2. The temperatures varied between 300 and 900 K, while the pressures were between 0.1 and 2.0 MPa. The results were compared with those obtained from the HITRAN database. HITRAN is a high-resolution transmission molecular absorption database. It is a compilation of spectroscopic parameters used to predict and simulate the transmission and emission of light from gaseous substances. The HITRAN database is recognised by many researchers, and is used in many different applications such as transmission simulations, fundamental laboratory spectroscopy studies and combustion physics [29]. Figure 5 shows that the molar absorption coefficient increases as the ambient pressure increases from 0.1 MPa to 1.0 MPa and changes slightly when the pressure level is above 1.0 MPa. The measured molar absorption coefficients for the different pressures and temperatures agreed well with the corresponding values in the HITRAN database.

The experimental results for the CO_2 absorption in the engine cylinder are shown in Figure 6. This figure indicates that the HCCI combustion process could be divided into two consecutive parts: a low-temperature reaction (LTR) region, and a high-temperature reaction (HTR) region; both parts were visible on the pressure trace and the rate of heat release curve. The LTR region was characterised by the low oxidation rate of the DME. We observed that the IR signal strength is affected by the in-cylinder pressure. We measured the IR detector voltage using an optical chopper to eliminate the effect of background radiation on the raw IR signal. The raw IR signal was stable as CO_2 was not absorbed during the compression stroke. CO_2 was formed in the HTR region. After the HTR region, the baseline of the IR signal rapidly increased and the transmissivity of the laser light decreased, due to the absorption of laser light with a wavelength of 4.3 μm by the CO_2 gas. These combined results indicate that the in-cylinder pressure, ROHR, IR signal and transmissivity due to CO_2 absorption are correlated.

3.2 Spatially integrated flame luminosity

To obtain a qualitative representation of the rate of combustion, we integrated the flame luminosity over the cross-sectional area of the engine cylinder. The spatial distribution of the flame luminosity was determined using numerical integration. For a continuous surface $Z = f(x,y), (x,y) \in \sigma$, the volume beneath it can be computed with

$$\iint_{(\sigma)} f(x,y)\,dxdy \tag{2}$$

Applying the method for numerical integration, this can be written as

$$\iint_{(\sigma)} f(x,y)\,dxdy = \lim_{\Delta x \to 0} \lim_{\Delta y \to 0} \sum_{i=0}^{m-1} \sum_{j=0}^{n-1} f(x_i, y_j) \Delta x \Delta y \approx \sum_{i=0}^{M-1} \sum_{j=0}^{N-1} f(x_i, y_j) \Delta x \Delta y \tag{3}$$

where M and N are the number of rows and columns of the computational matrix, respectively. In the actual computation, $\left(f(x_i, y_j) + f(x_i, y_{j+1}) + f(x_{i+1}, y_j) + f(x_{i+1}, y_{j+1}) \right) / 4$ was used instead of $f(x_i, y_j)$.

Raw two-dimensional images of the flame intensity in the HTR region are shown on the left-hand-side of Figures 7–9. These were obtained with a high-speed camera at a fixed equivalence ratio of 0.3, intake pressure 65 kPa and intake temperatures of 293 K, 303 K and

310 K. Combustion appeared as a blue flame; a luminescent flame from soot was not observed. The images on the right-hand-side of Figures 7–9 show the effects of post-processing. The post processing took into account the distribution of flame intensity. The image intensity before the start of mixture autoignition was subtracted from the image intensity during combustion. This eliminated the background light so that only the magnitude of the light emitted from the flame was plotted. There were marked differences between the flame intensities for weak (293 K), medium (303 K) and strong (310 K) combustion cycles. These differences arise from differences in the IR signal strength and the amount of light transmitted due to CO_2 absorption. Figure 7, which corresponds to graph (A) on Figure 6, shows very weak flame intensity. Figures 8 and 9, which respectively correspond to graphs (B) and (C) on Figure 6, show that the distributed reactions appeared to progress inhomogeneously. The inhomogeneity was due to temperature and concentration fluctuations. These observations are in agreement with previous results. Hultqvist et al. [7] used chemiluminescence images and spectra to investigate HCCI combustion processes fuelled using blends of n-heptane and isooctane. They observed that during high temperature heat release, the fuel/air mixture begins to autoignite at arbitrary points throughout the visible area. Dec et al. [30, 31] investigated HCCI isooctane chemiluminescence images obtained from a single-cylinder optical engine and a high-speed intensified camera. High-speed chemiluminescence images show that the HCCI combustion is a progressive process from the hot region to the cold region, even when the fuel and air are fully premixed before intake occurs. This indicates that HCCI combustion is not homogeneous. The authors suggested that the inhomogeneities derive primarily from the natural thermal stratification caused by heat transfer during compression and turbulent transport in the cylinder.

3.3 Time-resolved CO_2 absorption

We found that the laser light transmissivity was correlated with the heat release rate during the combustion process. Figure 10 shows that, for a number of experiments, the minimum light transmissivity gradually decreases as the maximum rate of heat release increases. R^2, the coefficient of determination, has a value 0.82494. This is a statistical measure indicating how well the regression line approximates the real data points. This trend shows the relationship between the in-cylinder pressure, the transmitted light and the energy release during the DME-HCCI combustion process.

Using the data for the transmissivity and absorption coefficient, the molar CO_2 concentration was calculated for different experimental conditions. Figure 11 shows a gradual increase in CO_2 concentration (B), calculated from absorption data, as the rate of heat release (A) increases during the in-cylinder DME combustion. The peak heat release rate in the LTR region is only slightly different to the rate in the HTR region. The similar levels of heat release in the LTR region occur due to the formation of formaldehyde and the high concentration of H_2O_2, which is further consumed. This facilitates the formation of OH radicals before high-temperature reactions are initiated. Westbrook [32] reported that the H_2O_2 decrease and the OH increase occurred almost simultaneously, and that H_2O_2 decomposition was the initiator of thermal ignition. However, Kuwahara and Ando [33] reported that the decrease in H_2O_2 started earlier than the OH increase, and that the rapid OH increase started during the final stages of this process. Nevertheless, both research groups agreed that the rapid OH increase occurred at the end of the thermal-ignition preparation region. Taking into account these findings, and the results of our experiments, we propose that the CO_2 concentration increases only when high-temperature reactions are initiated.

The newly developed CO_2 concentration measurement system, using QCL and optical fibre sensors, enabled us to measure the CO_2 concentration *in situ* during HCCI-DME combustion in a compression-expansion engine. Our results suggest that our CO_2 absorption detection technique gives rise to results that agree with general trends, where CO_2 formation is a product of hydrocarbon fuel combustion. We emphasise that categorising the experimental results by different combustion intensities (weak, medium and strong), as captured by high-speed camera imaging, allowed us to demonstrate that the CO_2 absorption behaviour was directly correlated with the transient in-cylinder combustion characteristics such as pressure, ROHR, light transmissivity and IR signal. Our future work will focus on measuring transient CO_2 concentrations under boosted engine conditions.

4. Conclusions

A new measurement technique was developed based on QCL and optical fibre sensors. Our technique enables the *in situ* measurement of transient CO_2 concentrations during DME-HCCI combustion. We draw the following conclusions:

1. Lambert–Beer's law was applied for the case of a single absorption line of CO_2. Using a constant volume vessel, the relationship between the ambient pressure, temperature and the CO_2 molar absorption coefficient was determined. The coefficient increased as the pressure increased up to 1.0 MPa, where the rate of increase slowed dramatically.

2. The laser light transmissivity was correlated with the heat release rate during the combustion process. In some experiments, the minimum light transmissivity decreased gradually as the maximum rate of heat release increased.

3. The time-resolved CO_2 absorption profiles during the DME–O_2–Ar mixture combustion under a range of conditions indicated that the CO_2 absorbance increases only in the high-temperature reaction region.

4. There were marked differences in the intensity of the emissions in different combustion cycles with identical initial conditions. The number, intensity, and size of hot spots in those cycles varied significantly due to combustion cyclic variations, leading to the observation of very inhomogeneous patterns.

The English in this document has been checked by at least two professional editors, both native speakers of English. For a certificate, please see:
http://www.textcheck.com/certificate/zaO8bB

References

[1] Takatsuto R, Igarashi T, Iida N. Auto-ignition and combustion of DME and n-Butane/air mixtures in homogeneous charge compression ignition engine. in: Proceedings of the 4th

International Symposium COMODIA 1998:185-90.

[2] Perrson H, Hultqvist A, Johansson B. Investigation of the early flame development in spark assisted HCCI combustion using high speed chemiluminescence imaging. SAE Paper 2007-01-0212; 2007.

[3] Flowers DL, Killingsworth NJ, Espinosa-Loza F, Martinez-Frias J, Aceves SM, Krstic M, Dibble R. Demonstrating Optimum HCCI Combustion with Advanced Control Technology. SAE Paper 2009-01-1885; 2009.

[4] Manente V, Zander C, Johansson B, Tunesta P, Cannella W. An advanced internal combustion engine concept for low emissions and high efficiency from idle to max load using gasoline partially premixed combustion. SAE Paper 2010-01-2198; 2010.

[5] Arcoumanis C, Bae C, Crookes R, Kinoshita E. The potential of di-methyl ether (DME) as an alternative fuel for compression-ignition engines: a review. Fuel 87; 2008:1014-30.

[6] Iida N. Combustion analysis of methanol-fueled active thermo-atmosphere combustion (ATAC) engine using a spectroscopic observation. SAE Paper 940684; 1984.

[7] Hultqvist A, Cristensen M, Johansson B, Richter M, Alden M. A study of the homogeneous charge compression ignition combustion process by chemiluminescence imaging. SAE Paper 1999-01-3680; 1999.

[8] Kim B, Kaneko M, Ikeda Y, Nakajima T. Detailed spectral analysis of the process of HCCI combustion. Proc Combust Inst 2002;29:671–677.

[9] Iijima A, Yoshida K, Shoji H. A study of autoignition in an HCCI engine by using light absorption and emission spectroscopy in: Proceedings of the 7th International Symposium COMODIA 2008: 297-303.

[10] Schultz C, Jeffries JB, Davidson DF, Kocj JD, Wolfrum J, Hanson RK. Impact of UV absorption by CO2 and H2O on NO LIF in high-pressure combustion applications. Proc Combust Inst 2002;29:2735–2742.

[11] Farooq A, Jeffries JB, Hanson RK. High-pressure measurements of CO2 absorption near 2.7 μm: Line mixing and finite duration collision effects. J Quant Spectrosc Radiat Transfer 2010;111:949-960.

[12] Hall MJ, Zuzek P. Fiber Optic sensor for time-resolved measurements of exhaust gas recirculation in engines. SAE Paper 2000-01-2865; 2000.

[13] Kawahara N, Tomita E, Ohtsuki A, Aoyagi Y. Cycle-resolved residual gas concentration measurement inside a heavy-duty diesel engine using infrared laser absorption. Proc Combust Inst 2011;33:2903–2910.

[14] Hall MJ, Zuzek P, Anderson RW. Fiber optic sensor for crank angle resolved measurements of burned gas residual fraction in the cylinder of an SI engine. SAE Paper 2001-01-1921;2001.

[15] Francqueville LD, Thirouard B, Ricordeau V. Measurement of residual gas fraction using IR absorption. SAE Paper 2006-01-3337; 2006.

[16] Grosch A, Wackerbarth H, Thiele O, Berg T, Beckmann L. Infrared spectroscopic concentration measurements of carbon dioxide and gaseous water in harsh environments

with a fiber optical sensor by using the HITEMP database. J Quant Spectrosc Radiat Transfer 2014;133:106-116.

[17] Sanders ST, Baldwin JA, Jenkins TP, Baer DS, Hanson RK, Diode-laser sensor for monitoring multiple combustion parameters in pulse detonation engines. Proc Combust Inst 2000;28:587–94.

[18] Mattison DW, Jeffries JB, Hanson RK, Steeper RR, De Zilwa S, Dec JE, Sjoberg M, Hwang W. In-cylinder gas temperature and water concentration measurements in HCCI engines using a multiplexed-wavelength diode-laser system: Sensor development and initial demonstration. Proc Combust Inst 2007;31:791–8.

[19] Schlosser TFE, Teichert H, Ebert V. In-situ-detection of potassium atoms in high-temperature coal-combustion systems using near-infrared-diode lasers. Spectrochimica Acta 2002;58:2347–59.

[20] Fernholz T, Teichert H, Ebert V. Digital, phase-sensitive detection for in situ diode-laser spectroscopy under rapidly changing transmission conditions. Applied Physics B: Lasers and Optics 2002;75:229–36.

[21] Rieker GB, Li H, Liu X, Liu JTC, Jeffries JB, Hanson RK, et al. Rapid measurements of temperature and H2O concentration in IC engines with a spark plug-mounted diode laser sensor. Proc Combust Inst 2007;31:3041–9.

[22] Kranendonk LA, Walewski JW, Kim T, Sanders ST. Wavelength-agile sensor applied for HCCI engine measurements. Proc Combust Inst 2005;30:1619–27.

[23] Rieker G, Jeffries J, Hanson R. Measurements of high-pressure CO2 absorption near 2.0mm and implications on tunable diode laser sensor design. Applied Physics B:Lasers and Optics 2009;94:51–63.

[24] Eng JA. Characterization of pressure waves in HCCI combustion. SAE Paper 2002-01-2859; 2002.

[25] Dubreuil A, Foucher F, Mounaim-Rousselle C, Dayma G, Dagaut P. HCCI combustion: Effect of NO in EGR. Proc Combust Inst 2007;31:2879–2886.

[26] Ebrahimi K and Koch CR. HCCI combustion timing control with variable valve timing. American Control Conference (ACC) Washington, DC, USA, June 17-19, 2013

[27] Saigaonkar H, Nazemi M, Shahbakhti M. Sequential model for residual affected HCCI with variable valve timing. SAE Paper 2015-01-1748; 2015.

[28] Kazarinov RF, Suris RA. Possibility of amplification of electromagnetic waves in a semiconductor with a superlattice. Fizika i Tekhnika Poluprovodnikov 1971;5:797–800.

[29] Rothman LS, Rinsland CP, Goldman A, S.T. Massie ST, Edwards DP, Flaud JM, Perrin A, Camy-Peyret C, Dana V, Mandin JY, Schroeder J, Mccann A, Gamache RR, Wattson RB, Yoshino K, Chance KV, Jucks KW, Brown LR, Nemtchinov V, Varanasi P. The HITRAN molecular spectroscopic database and HAWKS (HITRAN atmospheric workstation): 1996 Edition. J. Quant. Spectrosc. Radiat. Transfer 1998;60:665-710.

[30] Dec JE, Hwang W and Sjoberg M. An investigation of thermal stratification in HCCI engines using chemiluminescence imaging. SAE Paper 2006-01-1518, 2006.

[31] Hwang W, Dec J and Sjoberg M. Spectroscopic and chemical-kinetic analysis of the phases

of HCCI autoignition and combustion for single- and two-stage ignition fuels. Combust Flame 2008;154, 387–409.
[32] Westbrook CJ. Chemical kinetics of hydrocarbon ignition in practical combustion systems. Proc Combust Inst 2000;28:1563-77.
[33] Kuwahara K, Ando H. Role of heat accumulation by reaction loop initiated by H_2O_2 decomposition for thermal ignition. SAE Paper 2007-01-0908; 2007.

LIST OF TABLES

Table 1. Test engine specification

LIST OF FIGURE CAPTIONS

Figure 1. Schematics of a compression-expansion test engine.

Figure 2. Center wavelength of Quantum Cascade Laser and absorption line of CO_2

Figure 3. (A) Position of the optical spark-plug sensor on the engine cylinder head. (B) Schematics of the optical spark-plug sensor design.

Figure 4. Rate of maximum in-cylinder pressure rise for different combustion cycles.

Figure 5. Molar absorption coefficient at different temperatures and pressures.

Figure 6. IR signal strength and light transmissivity during DME-HCCI engine combustion. (A) Weak combustion intensity. (B) Moderate combustion intensity. (C) Strong combustion intensity.

Figure 7. Left-hand-side: sequential raw images of DME-HCCI combustion with weak combustion intensity. Images were obtained using a high-speed colour camera at P_{in}=65 kPa, T_{in}=293 K and ϕ=0.3. Right-hand-side: Background-subtracted, post-processed images with light intensity distribution.

Figure 8. Left-hand-side: sequential raw images of DME-HCCI combustion with moderate combustion intensity. Images were obtained using a high-speed colour camera at P_{in}=65 kPa, T_{in}=303 K and ϕ=0.3. Right-hand-side: Background-subtracted, post-processed images with light intensity distribution.

Figure 9. Left-hand-side: sequential raw images of DME-HCCI combustion with strong combustion intensity. Images were obtained using a high-speed colour camera at P_{in}=65 kPa, T_{in}=310 K and ϕ=0.3. Right-hand-side: Background-subtracted, post-processed images with light intensity distribution.

Figure 10. Cycle-resolved correlation of maximum ROHR with minimum light transmissivity.

Figure 11. Crank angle-resolved ROHR and CO_2 concentration.

Table 1

Click here to download high resolution image

Bore	78 mm
Stroke	85 mm
Connecting rod length	153 mm
Displacement volume	406.2 cm^3
Compression ratio	9.0:1
Combustion chamber	Pancake type
Engine speed	600 rpm
Valve closure time	180 deg. BTDC

Figure 1
Click here to download high resolution image

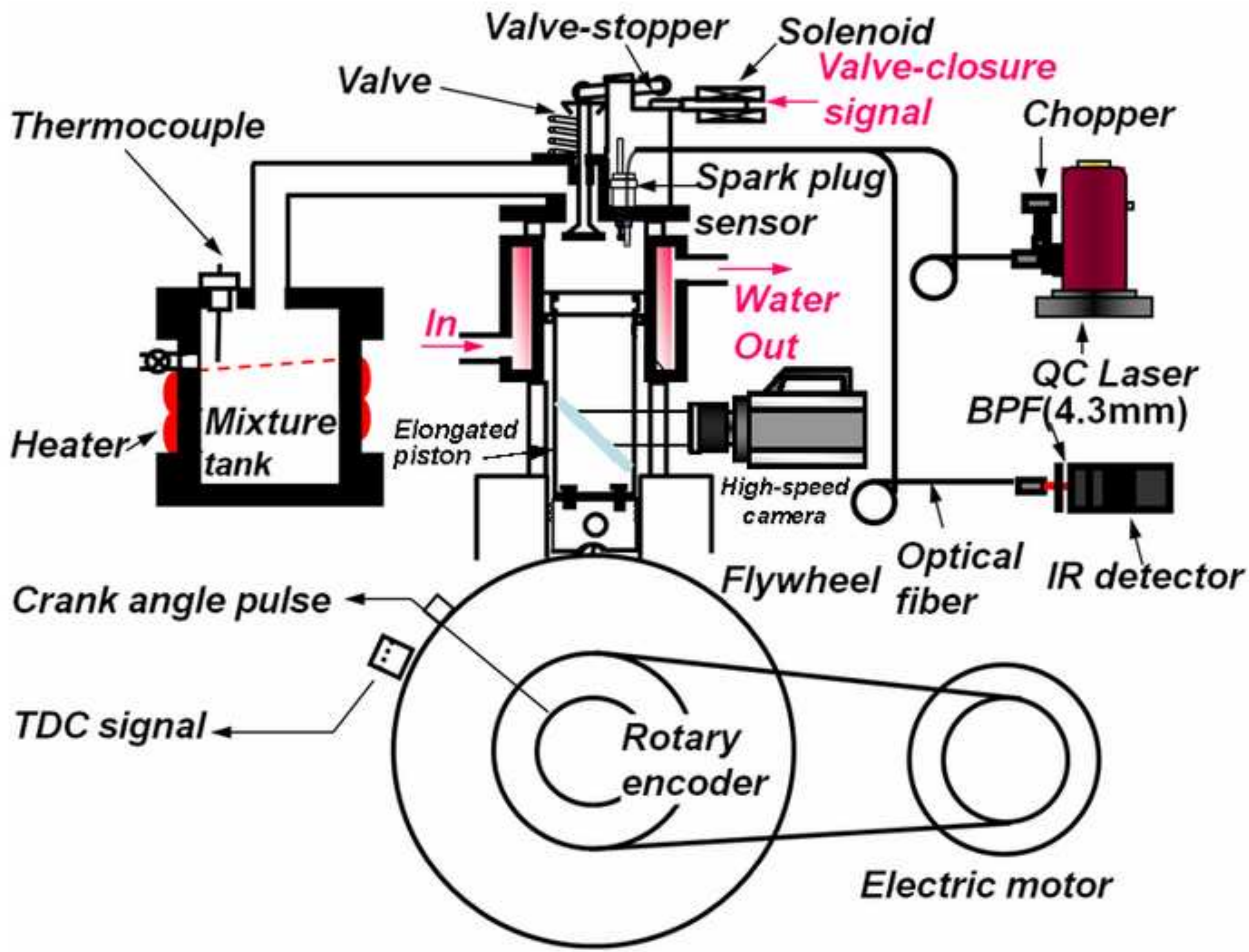

Figure 2

Click here to download high resolution image

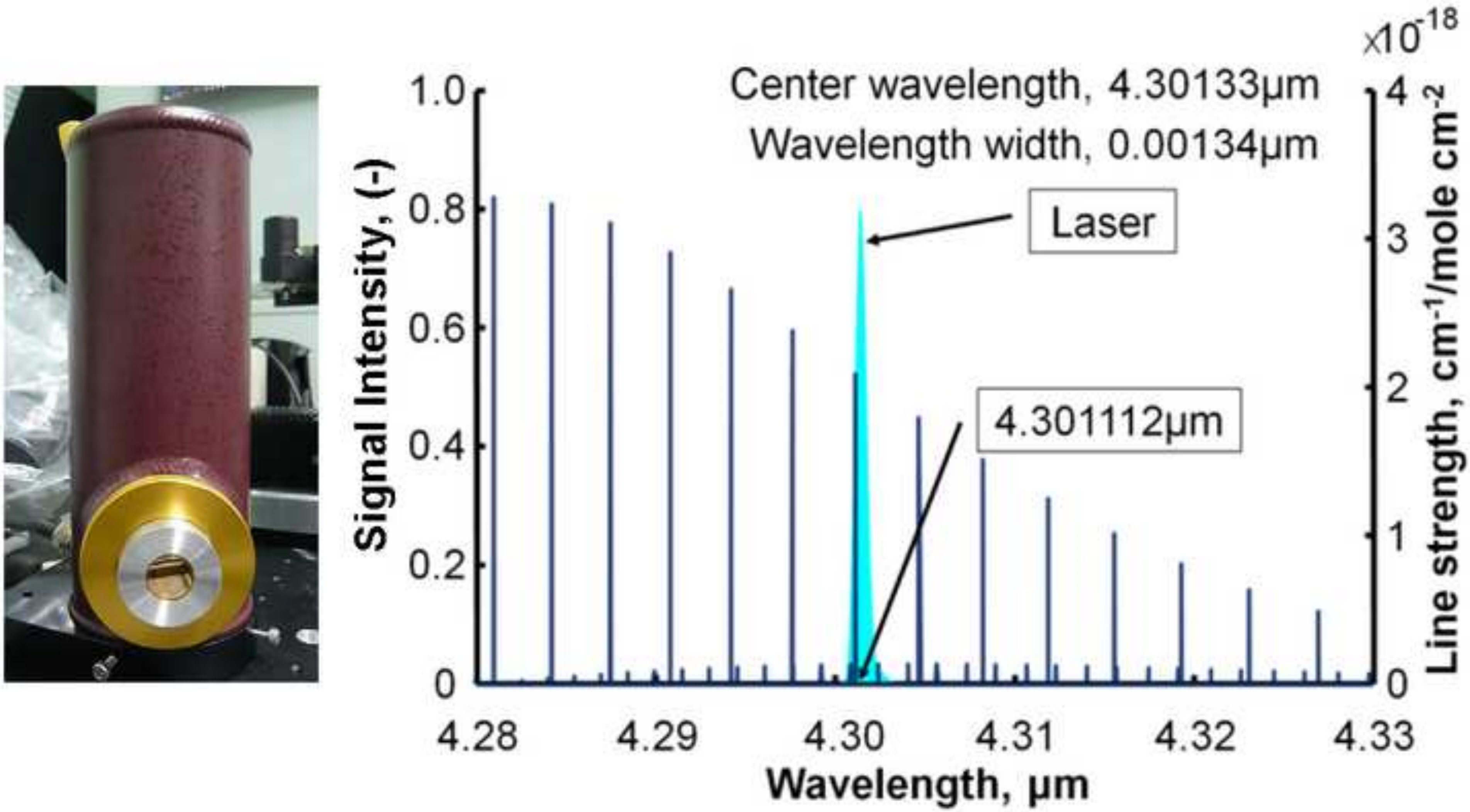

Figure 3
Click here to download high resolution image

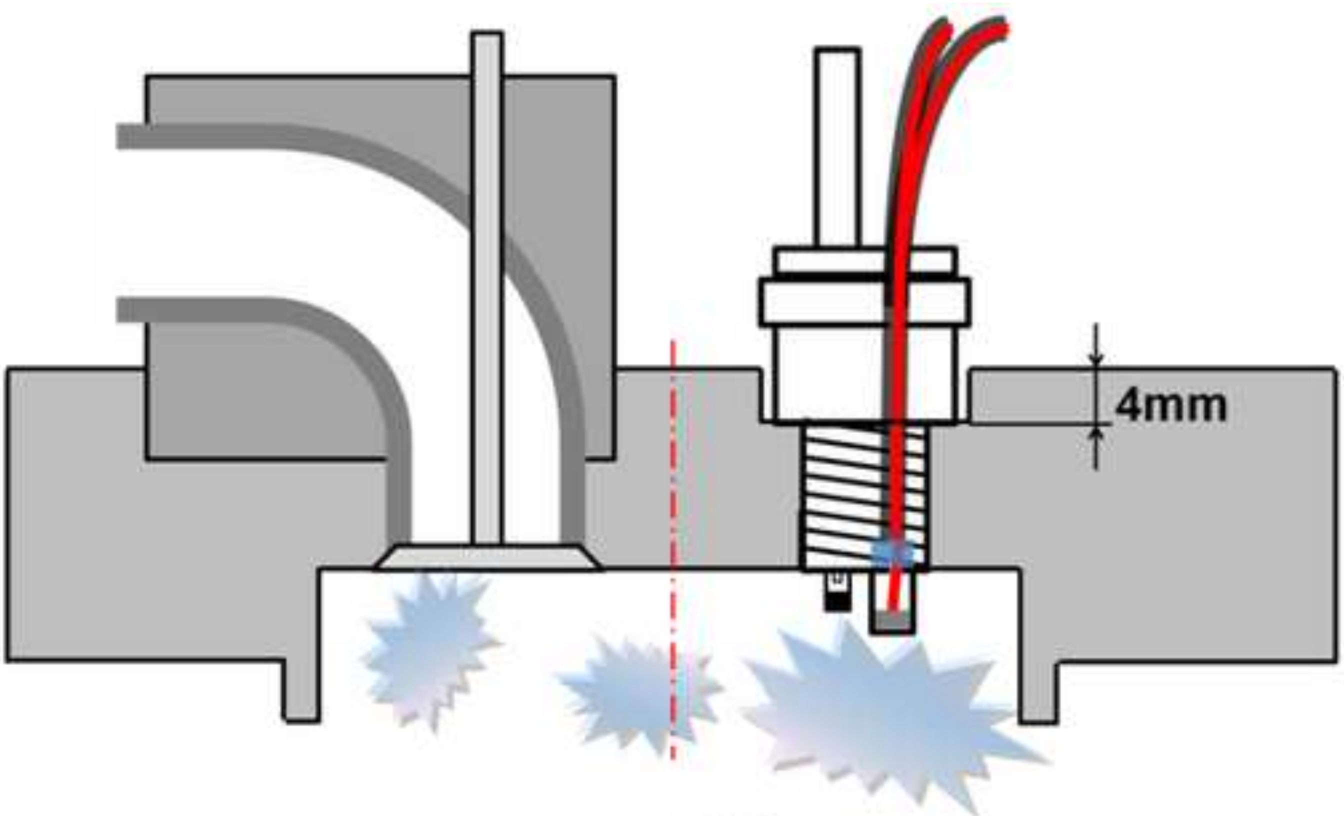

(A)

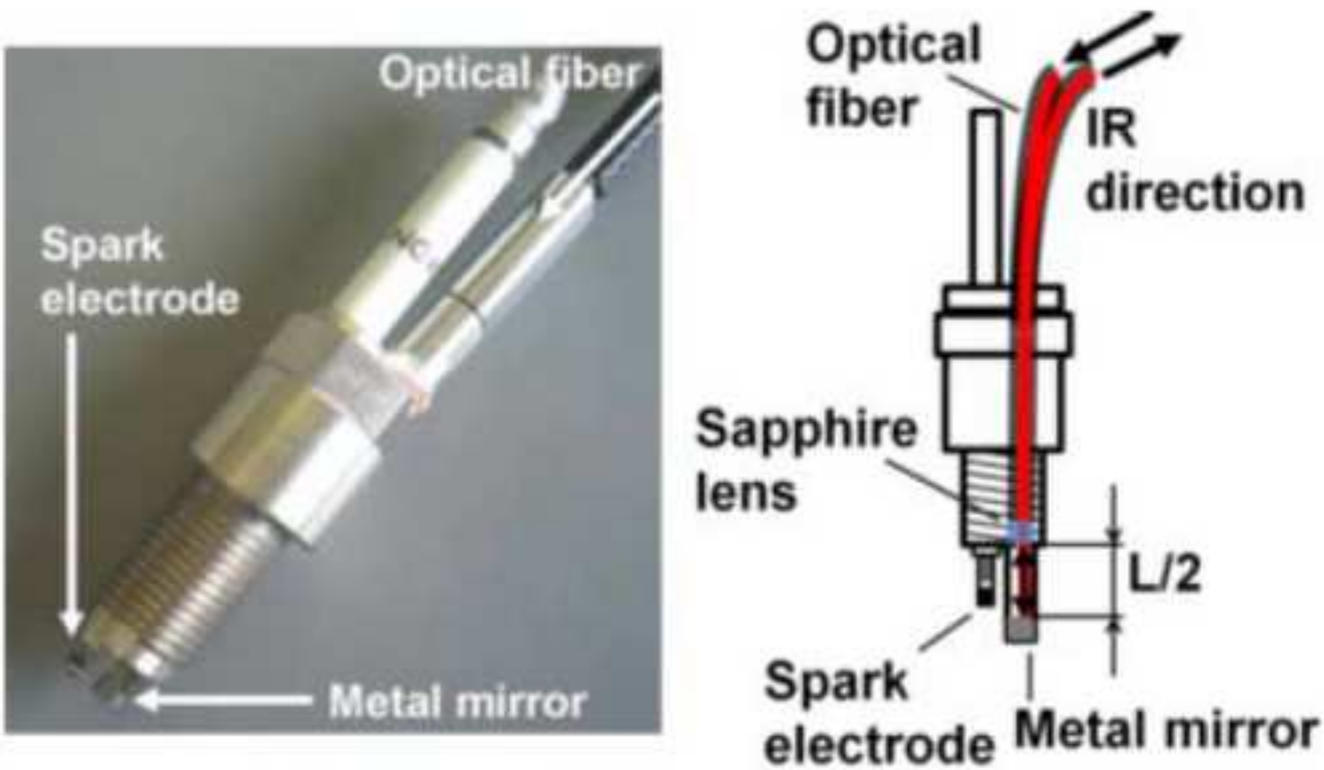

(B)

Figure 4

Click here to download high resolution image

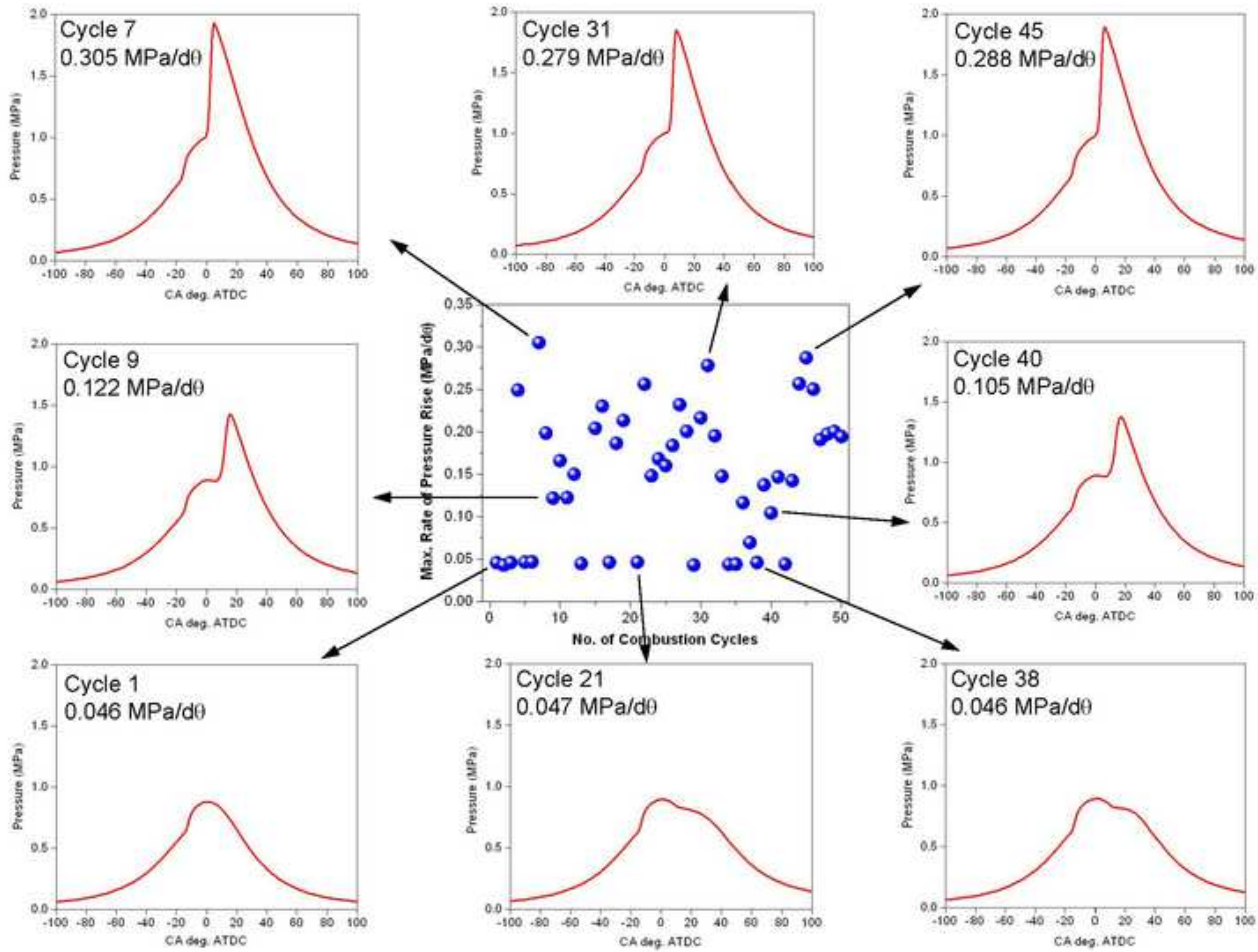

Figure 5

Click here to download high resolution image

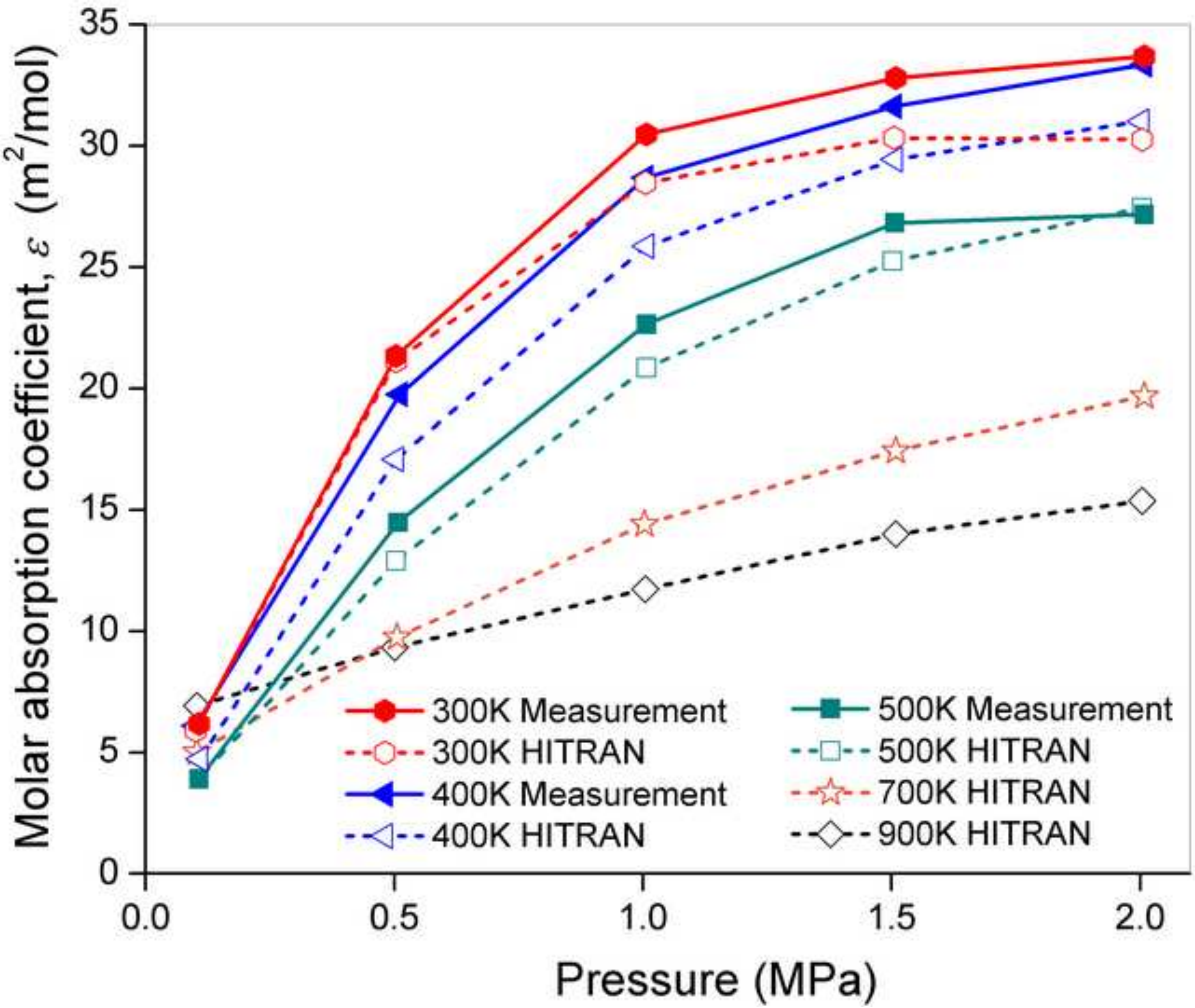

Figure 6
Click here to download high resolution image

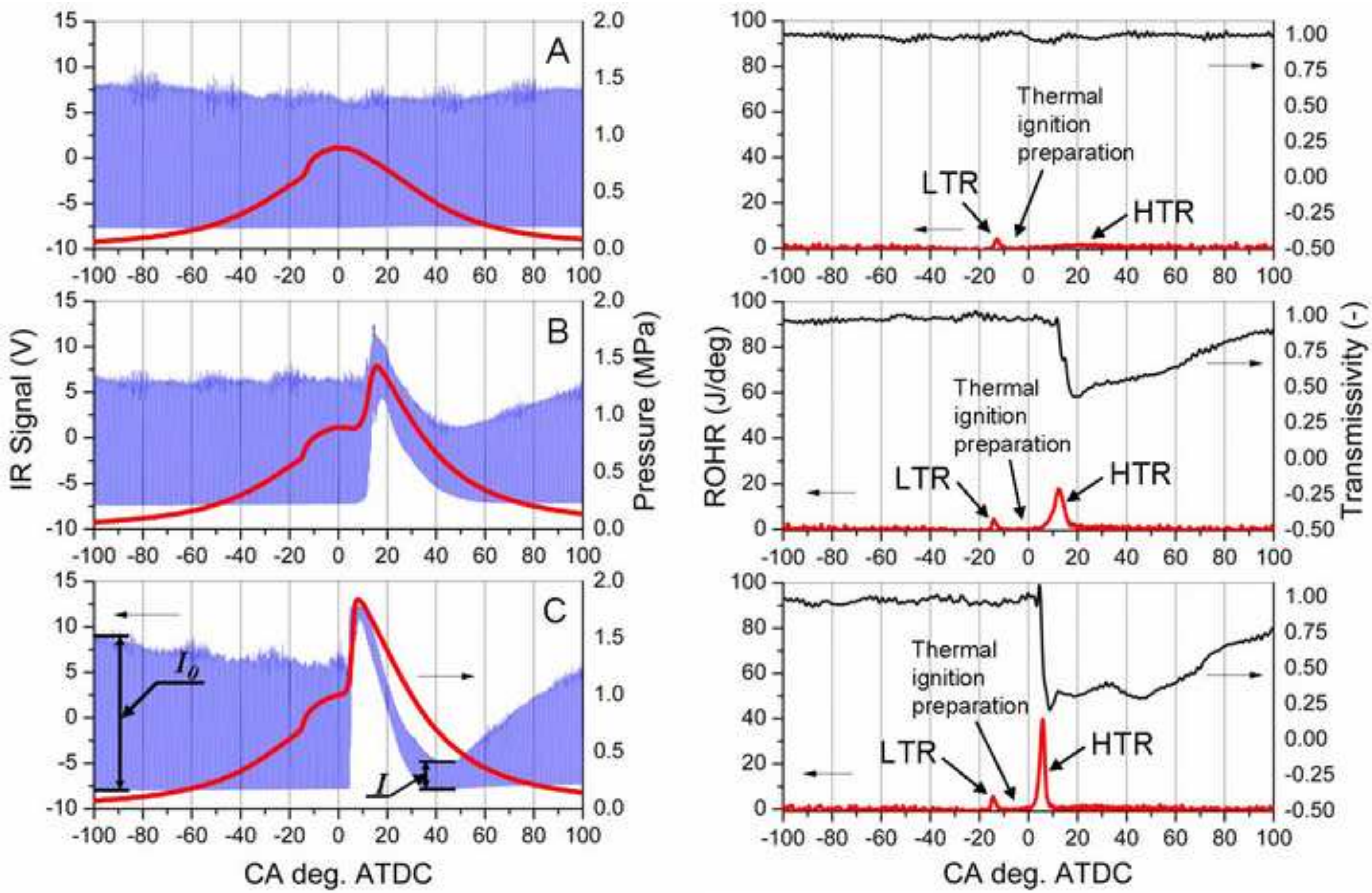

Figure 7
Click here to download high resolution image

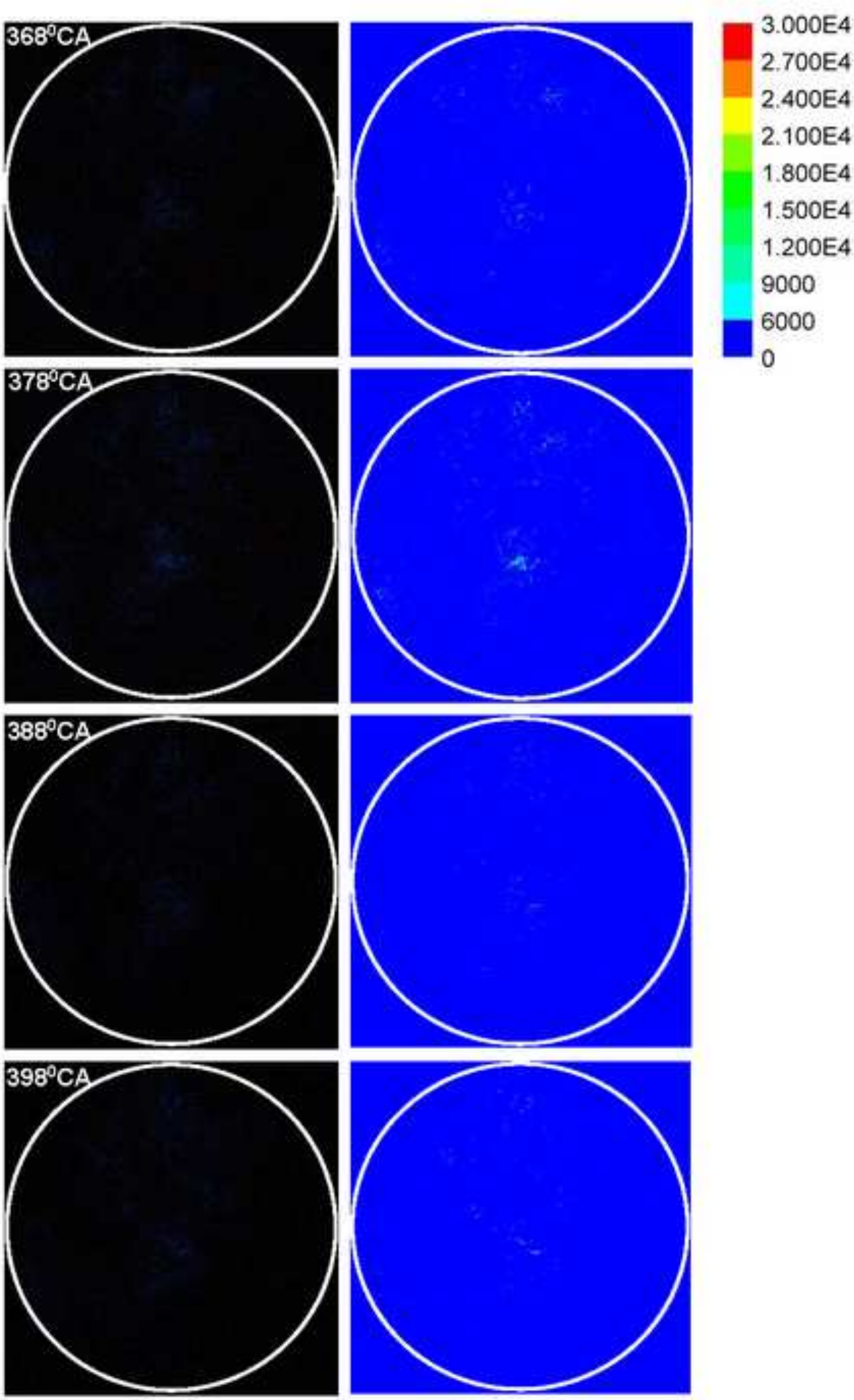

(A)

Figure 8
Click here to download high resolution image

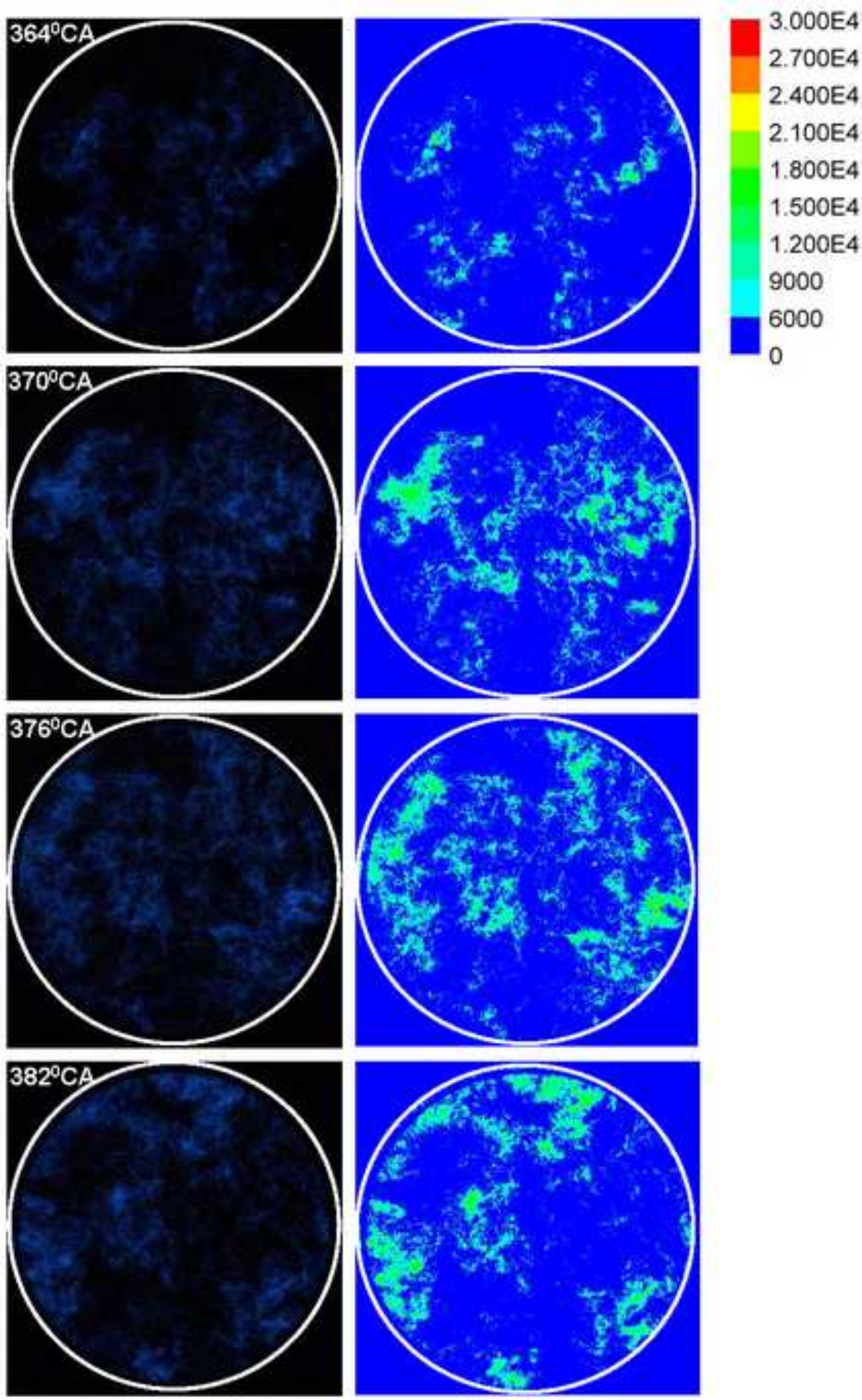

(B)

Figure 9
Click here to download high resolution image

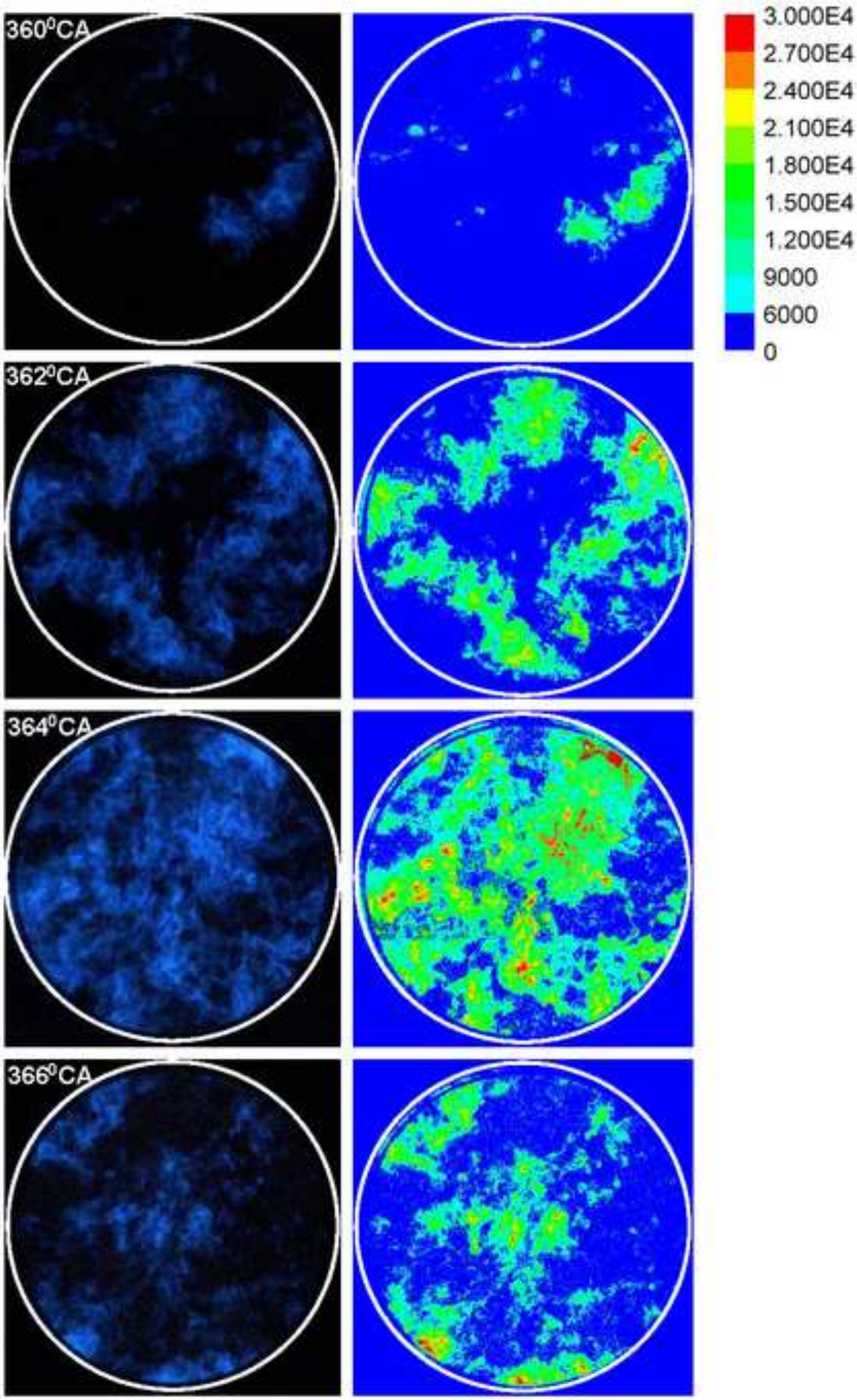

(C)

Figure 10

Click here to download high resolution image

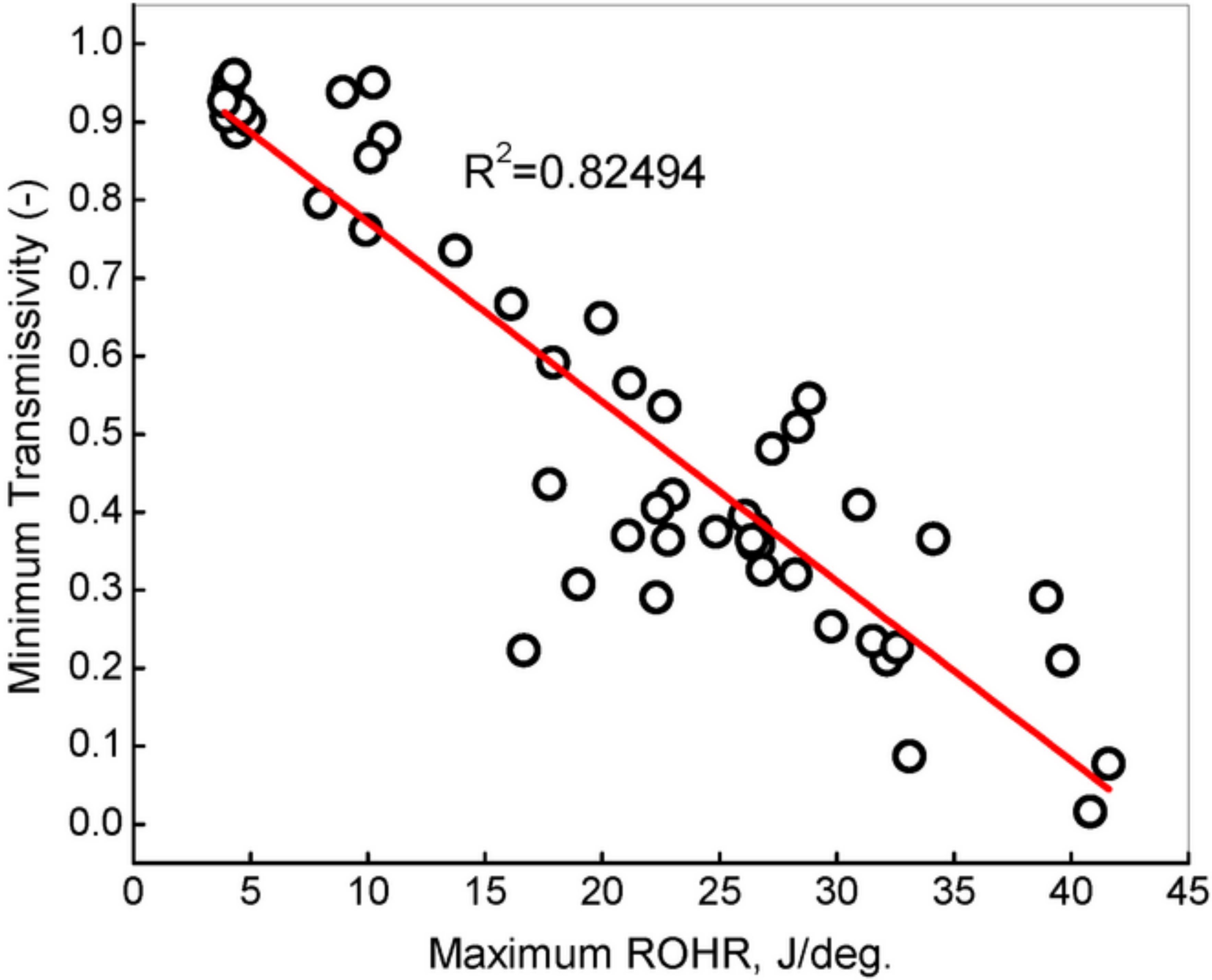

Figure 11
Click here to download high resolution image